J Appl Electrochem (2009) 39:197–204
DOI 10.1007/s10800-008-9653-9

ORIGINAL PAPER

Carbon-supported manganese oxide nanoparticles as electrocatalysts for oxygen reduction reaction (orr) in neutral solution

I. Roche · K. Scott

Received: 15 May 2008 / Accepted: 18 August 2008

Abstract Manganese oxides (MnO_x) catalysts were chemically deposited onto various high specific surface area carbons. The MnO_x/C electrocatalysts were characterised using a rotating disk electrode and found to be promising as alternative, non-platinised, catalysts for the oxygen reduction reaction (ORR) in neutral pH solution. As such they were considered suitable as cathode materials for microbial fuel cells (MFCs). Metal [Ni, Mg] ion doped MnO_x/C, exhibited greater activity towards the ORR than the un-doped MnO_x/C. Divalent metals favour oxygen bond splitting and thus orientate the ORR mechanism towards the 4-electron reduction, yielding less peroxide as an intermediate.

Keywords Oxygen reduction reaction · Microbial fuel cell · Manganese oxides · Neutral pH · Electrocatalysis

1 Introduction

Poor kinetics of the oxygen reduction reaction electrocatalysts (ORR) at neutral pH and low temperatures can hinder the performance and development of fuel cells under these conditions [1–3]. This is especially the case in, for example, microbial fuel cells (MFCs) where low power performance would necessitate high capital cost, especially for the electrodes. Platinum is known to be the best catalyst for the ORR in acid and alkaline media [4]. However, for simple cost reasons, non-platinised materials represent a necessary alternative. There has been limited research into catalysts for the ORR in neutral solution and very few platinum free catalysts have been studied. Electrochemical studies have been carried out in neutral solution with metal tetramethoxyphenylporphyrin (TMPP), CoTMPP and FeCoTMPP, and metal phthalocyanine (Pc), FePc, CoPc and FeCuPc, supported on Ketjenblack (KJB) carbon: the FePc/KJB catalysts exhibited very good activity towards the ORR [5].

Manganese oxides are promising as catalysts for ORR in neutral media [6]. Electrochemical properties of manganese oxides have been studied in alkaline media, but very few studies have been carried out at neutral pH [7, 8]. Chartier et al. described rather good activity of MnO_x in neutral and slightly acid media, together with the role of the Mn^{IV}/Mn^{III} redox couple on the 4 and 2 electron oxygen reduction mechanisms [7, 8]. However these studies concerned mixed valency spinel $Cu_xMn_{3-x}O_4$ oxides. No studies, to our knowledge, have been carried out on MnO_x/C-based materials as electrocatalysts for the ORR at neutral pH.

Carbon-supported manganese oxides nanoparticles were found to exhibit good ORR activity in alkaline media [9–13]. In addition the doping of MnO_x/C by the divalent ions Ni^{II}, Mg^{II} or Ca^{II}, was found to be extremely promising, since the Me-MnO_x/C catalysts exhibited ORR activity close to that of a benchmark Pt/Vulcan XC72 from E-Tek [12, 13]. We have characterised the ORR activity of such MnO_x/C-based catalysts in neutral pH solution.

The present work has evaluated the activity of carbon-supported MnO_x electrocatalysts towards the ORR at neutral pH for use as cathode material in MFCs. In particular the influence of the doping of MnO_x/C-based electrocatalysts and the carbon support, on the ORR

I. Roche (✉) · K. Scott
School of Chemical Engineering and Advanced Materials,
University of Newcastle upon Tyne, Newcastle upon Tyne NE1
7RU, UK
e-mail: rochivan@yahoo.fr

activity of the carbon-supported manganese oxide nanoparticles, was studied. Results were compared to those of a benchmark 20% by weight (20 wt.%) Pt/Vulcan XC72 from E-Tek. The ORR mechanism on MnO_x/C-based catalysts was also studied.

2 Experimental

2.1 Synthesis of MnO_x/C materials

The manganese oxide nanoparticles were chemically deposited onto the carbon substrate as follows [10, 11]: 4 g of carbon was mixed with a 70 cm^3 (mL) of an aqueous solution containing 10 mmol (mM) of $MnSO_4$ (Aldrich). The suspension was maintained at a controlled temperature (80 °C) for 20 min under magnetic stirring, in order to allow impregnation of the carbon by manganese sulphate. A 300 mL aqueous solution, containing 33 mmol of $KMnO_4$ (Merck), previously heated at controlled 80 °C, was then gradually added to the agitated suspension. $MnSO_4$ is oxidized by the permanganate in the presence of the carbon according to the chemical reaction [14]:

$$\begin{aligned} &2KMnO_4 + 3MnSO_4 + 2H_2O \\ &\quad \rightarrow 5MnO_2 + 2H_2SO_4 + K_2SO_4 \end{aligned} \tag{1}$$

The reaction medium was maintained at 80 °C under agitation for 15 min and then washed, filtered and dried at 100 °C for approximately 10 h. The corresponding mass ratios in the obtained MnO_x/C material were 4.0 g of C to 2.4 g of Mn. The specific surface areas of Vulcan XC72 (called Vulcan) and Monarch 1000 (called Monarch), were 240 and 300 $m^2\ g^{-1}$, respectively [14]. The suspension was maintained at a controlled temperature (80 °C) for 15 min and then filtered and dried at 100 °C. Similar oxidations, using potassium permanganate, were performed on the carbon supports alone, and these are named as Vulcan $XC72_{ox}$ or $Monarch1000_{ox}$.

To prepare the Ni, Mg or Ca-doped catalysts, a solution (0.01 mol) of $Ni(NO_3)_2 \cdot 6H_2O$ (Aldrich), $Mg(NO_3)_2 \cdot 6H_2O$ or $Ca(NO_3)_2 \cdot 4H_2O$ (Aldrich) was added prior to the permanganate addition [10].

All MnO_x/C-based catalysts should exhibit a Mn loading of ca. 20 wt.%, and Me loadings of ca. 7, 3 and 4 wt.% for Me = Ni, Mg and Ca, respectively, at the time of their synthesis according to previous reports of this preparation method[10]. If all the Mn is present as MnO_2, the materials should have a MnO_2 loading of ca. 30 wt.%. Previous papers [10, 13] have shown evidence that the manganese oxides are well dispersed over the carbon support as MnO_2. However, X-ray diffraction (XRD) experiments were undertaken for the MnO_x/C-based materials. Using the manganese loading values, the current densities with respect to the mass of active materials were calculated. A more precise physico-chemical characterisation of the MnO_x/C-based materials is part of on-going work.

2.2 XRD characterisation

The chemistry of MnO_x particles supported on carbon black is complex. In order to determine the MnO_x crystallographic structures on the carbon, X-ray diffraction (XRD) for all our MnO_x/C-based materials was performed on a Panalytical (ex-Philips) X'Pert Pro MPD (multi purpose diffractometer) equipped with a diffracted-beam monochromator, using Cu Kα radiation. The XRD characterisations were carried out in the *Chemical and Materials Analysis Services*, Sage Faculty, University of Newcastle (United Kingdom).

2.3 Materials and electrodes

Glassy carbon tips (diameter, φ 3.0 mm, 0.071 $cm^2_{geom.}$) were used as catalyst substrates to characterise the active layers of the catalysts. As described previously [12, 13], each active layer was deposited from an ink containing 25 mg of MnO_x/C or Me-MnO_x/C (Me = [Ni, Mg, Ca]) powder, 1 cm^3 of water, 0.6 cm^3 of propan-2-ol and of PTFE solution (60 wt.%, Aldrich). After homogenisation by sonication, a 0.002 cm^3 drop of the ink was deposited onto the glassy carbon electrode and solvents were evaporated at room temperature. The resulting porous active layer (containing ca. 14 wt.% PTFE on the basis of the dry materials) was then heat treated at 100 °C for 15 min to ensure its mechanical stability. A rotating disc electrode (Autolab, Netherlands) was used to evaluate the electrochemical activity of the MnO_x/C materials. All solutions were prepared with de-ionised water.

2.4 Electrochemical cells

The electrochemical tests were performed in 0.1 M Na_2SO_4 solution in a three-electrode glass cell. The initial pH was measured at ca. 7. A phosphate buffer medium was not used as this would have been potentially detrimental to the MnO_2 catalyst activity. A platinum foil was used as the counter electrode, the RDE as working electrode and the reference was a Ag/AgCl (sat) electrode ($E^\circ = +0.197$ V vs. SHE). All potentials are referred to the standard hydrogen electrode (SHE). Voltammetry was conducted using a computer-controlled potentiostat (Sycopel Scientific LTD, England). “Blank” experiments under nitrogen (BOC, England) were performed to characterise the active layers in terms of their stability in the ORR potential range. ORR voltammetry was carried out after oxygen (BOC, England) saturation of the electrolyte and the oxygen saturation concentration was maintained by O_2 bubbling in the solution. The solution temperature was thermostated at 25 (±1) °C. Successive ORR voltammograms were recorded on the MnO_x/C-based active layers (immobilized as the porous active layer on the glassy-carbon disk) from +0.7 V to −0.5 V (vs. SHE) at quasi-steady-state conditions (1 mV s^{-1}) for various RDE speeds of rotation. Prior to each voltammetric sweep the potential was maintained at a starting potential, +0.7 V vs. SHE, for 2 min, to ensure identical initial surface-states of all active layers.

3 Results and discussion

3.1 XRD results

XRD spectra (Fig. 1) revealed the diagnostic interlayer reflection typical for γ-MnO_2 [15] for the MnO_x/C-based materials for both carbon supports (Vulcan or Monarch). The XRD patterns did not reveal segregated nickel, magnesium or calcium domains, indicating that the divalent metals were inserted into the manganese oxide crystal lattice: true metal doping. The XRD peak at $2\theta = 36.8°$ was moved to a lower angle with doping; indicating metal insertion between the manganese oxide layers (Fig. 1), in agreement with previous reports [11, 13]. A volume average diameter of ca. 10 nm of the manganese oxide nanocrystallites (L_v) was estimated, starting from the XRD spectra (peaks $2\theta = 36.8°$ and 66.2° considered) and by considering the classical Scherrer equation [16]. However, TEM images are also required to confirm the previous XRD results and to estimate the particle size distribution of the MnO_2 particles dispersed over the carbon support. This is part of on-going work.

3.2 Proton insertion

Cyclic voltammograms obtained in N_2-saturated 0.1 M Na_2SO_4 solution (pH ca. 7), for MnO_x/C materials were stable on potential cycling between the second and twentieth cycles (Fig. 2): from +1.2 to +0.6 V vs. SHE. The material underwent reduction of metastable oxides, as revealed by the reduction peak around +0.87 V vs. SHE, corresponding to Eq. 2 [17]:

$$MnO_2 + H_2O + e^- = MnOOH + OH^- \qquad (2)$$

The peak potential was in agreement with that found in the Pourbaix diagram. Proton insertion (2) is followed by the 1-electron reduction of MnOOH yielding Mn^{2+} ions. This reduction is, however, strongly limited by resistive effects due to the low conductivity of MnOOH. As a consequence, MnOOH is partially dissolved in the electrolyte.

The catalytic activity of MnO_x/C materials has been shown to decrease upon potential cycling in alkaline medium; proton insertion thus being not totally reversible [12, 13]. The manganite (MnOOH) formed was quite soluble in alkaline medium and easily dissolved into the solution [18], the catalytic activity associated with the peak currents being then lost upon cycling. It has been shown that inclusion of divalent metal ions favoured stabilisation of Mn^{IV}/Mn^{III} species in alkaline medium, proton insertion then being reversible [13]. In contrast to experiments carried out in alkaline medium, cyclic voltammograms for MnO_x/C-based catalysts at neutral pH showed very stable electrocatalytic activity even for un-doped MnO_x/C catalysts, as there was little, if any, dissolution of MnOOH in neutral electrolyte. The experimental results were very

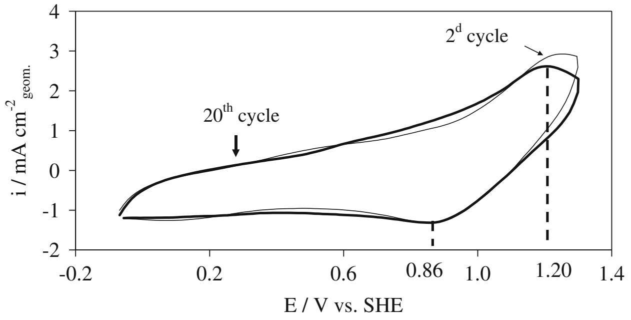

Fig. 2 Cyclic voltammograms for the MnO_x/Vulcan catalyst. 2^{d} (black) and 20th (gray) cycles, N_2-saturated 0.1 M Na_2SO_4 solution (pH ca. 7), at 25 °C, scan rate 0.1 V s^{-1}, speed of rotation $\Omega = 0$

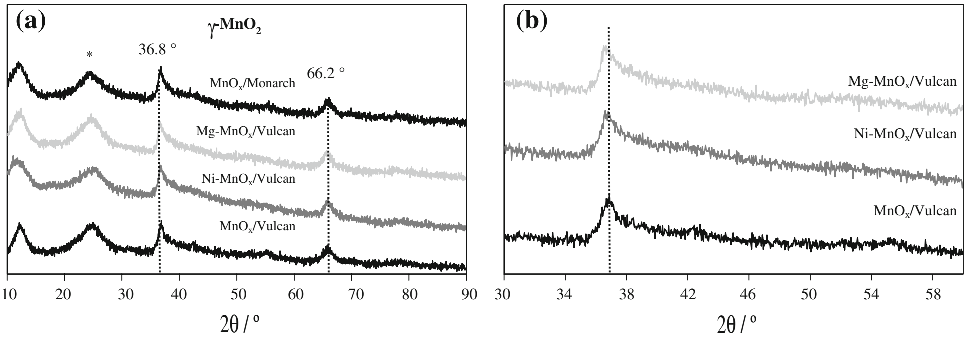

Fig. 1 (**a**) XRD spectra of MnO_x/Vulcan, Ni-MnO_x/Vulcan, Mg-MnO_x/Vulcan, and MnO_x/Monarch. The γ-MnO_2 phase is apparent (considered peaks: $2\theta = 36.8°$ and 66.2°. *diffraction peak of the carbon support. (**b**) $2\theta = 36.8°$ peak, considered for the MnO_x/Vulcan-based materials

repeatable. This very good stability suggests there was no loss of active material in neutral pH solution.

3.3 ORR activity

Successive voltammogramms obtained in oxygen-saturated, 0.1 M Na_2SO_4 solution (pH ca. 7) for the MnO_x/C active layers deposited on the RDE are shown in Fig. 3a, for MnO_x/Monarch. Similar voltammogramms were obtained for carbons (C_{ox}), previously oxidised by permanganate, to determine the influence of the carbon support on electrochemical activity (see the example of the carbon $Monarch_{ox}$ at 2,500 rpm, Fig. 3a). The pure Faradaic current for the ORR was obtained after subtraction of the *blank* current under nitrogen obtained under the same voltammetry conditions at which proton insertion occurs. The electrolyte was not buffered. During proton insertion, changes in the interfacial H^+ concentration could consequently be in the proximity of the active layer surface, especially for such MnO_x/C-based materials having a high specific surface area. In the coulombic charge regions the *blank* current were 10 to 20 times lower than currents under O_2. The ORR currents were then not significantly affected by possible interfacial pH variations. The current densities were limited, especially at high current densities, by oxygen diffusion in the solution and in the active layer, following the equation:

$$1/\left|i_{exp.}\right| = 1/|i_k| + 1/\left|i_l^{diff.solution}\right| + 1/\left|i_l^{diff.activelayer}\right| \qquad (3a)$$

$$1/\left|i_{exp.}\right| = 1/|i_k| + 1/\left(B\Omega^{1/2}\right) + 1/\left|i_l^{diff.activelayer}\right| \qquad (3b)$$

where,

$$B = 0.620\ n\ FC_{O2}D_{O2}^{2/3}\nu^{-1/6} \qquad (4)$$

is the Levich slope, $i_{exp.}$ is the measured current density at a given potential and revolution speed (Ω/rad s^{-1}) of the RDE, i_k the ORR kinetic current density, i_l the ORR limiting current density in the solution, n the number of exchanged electrons, F the Faraday constant (96,487 °C mol^{-1}). D_{O2} is the diffusion coefficient of O_2 in 0.1 M Na_2SO_4 aqueous solution, ν is the kinematic viscosity of the solution and C_{O2} is the oxygen concentration in the O_2-saturated solution.

Under air the oxygen solubility is 6 mg L^{-1} for seawater at 25 °C. It is then accordingly approximately 1.9×10^{-6} mol cm^{-3} for O_2-saturated seawater. The kinematic viscosity of the aqueous electrolyte is ca. 0.01 $cm^2\ s^{-1}$ at 25 °C and the oxygen diffusion coefficient D_{O2} is ca. 1.9×10^{-5} $cm^2\ s^{-1}$. Using these values, $B \approx 0.1$ n (mA cm^{-2} $rad^{-1/2}$ $s^{1/2}$).

The classical Tafel representations of the kinetic current densities in the ORR potential range for our MnO_x/C-based catalysts (see the example of $Monarch_{ox}$, MnO_x/Monarch and Ni-MnO_x/Monarch) is shown in Fig. 3b. The current

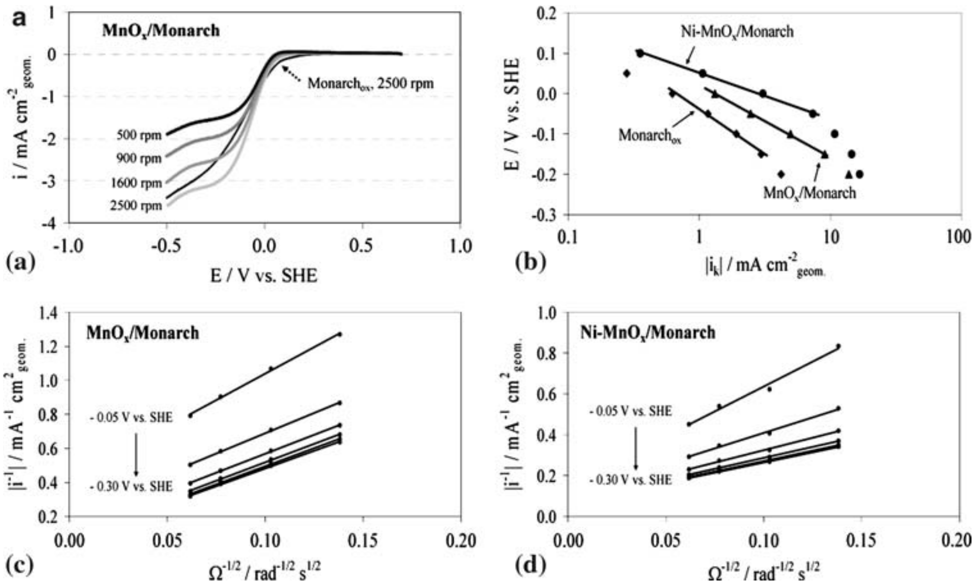

Fig. 3 (**a**) Voltammograms for the MnO_x/Monarch catalyst at different RDE rotation rates (500, 900, 1,600 and 2,500 rpm). Currents corrected for the blank, and for $Monarch_{ox}$, previously oxidized. O_2-saturated 0.1 M Na_2SO_4 solution at 25 °C, 0.001 V s^{-1}. (**b**) Corresponding Tafel plots, in the low current densities range, for Ni-MnO_x/Monarch ($b = -0.113$ V dec^{-1}), MnO_x/Monarch ($b = -0.177$ V dec^{-1}) and $Monarch_{ox}$, previously oxidized ($b = -0.161$ V dec^{-1}). The currents were corrected for O_2 diffusion in the solution and in the active layer. (**c**) Koutecky-Levich plots for MnO_x/Monarch at different potentials: −0.05, −0.10, −0.15, −0.20, −0.25 and −0.30 V vs. SHE. (**d**) Koutecky-Levich plots for Ni-MnO_x/Monarch at the same ORR potentials

Table 1 Kinetic parameters for the ORR in O_2-saturated 0.1 M Na_2SO_4 at 25 °C—corrected for oxygen diffusion in solution and the active layer. Potentials at current on-set, kinetic current densities at 0 V vs. SHE, corresponding mass activities (MA), based on the mass of platinum (Pt/C) or manganese dioxide (un-doped and doped)

Catalysts	$E_{on\text{-}set}$/V vs. SHE	i_k/mA $cm^{-2}{}_{geom.}$	MA/A $g^{-1}_{ptorMnO_2}$	b/V dec^{-1}
MnO_x/Vulcan	+0.29	0.6	**4**	−0.134
Ni-MnO_x/Vulcan	+0.33	1.3	**9**	−0.335
Mg-MnO_x/Vulcan	+0.28	0.7	**5**	−0.305
Ca-MnO_x/Vulcan	+0.18	0.2	**2**	−0.129
MnO_x/Monarch	+0.25	1.3	**9**	−0.177
Ni-MnO_x/Monarch	+0.26	2.8	**19**	−0.113
Pt/Vulcan (E-Tek)	+0.49	18.0	100	−0.213

densities were mass transfer corrected for the diffusion of oxygen in the solution, using the classical [19] Koutecky-Levich model (see Figs. 3c, d for MnO_x/Monarch and Ni-MnO_x/Monarch, respectively). The current densities were also corrected for the diffusion of oxygen in the active layer using the macro-homogeneous model [20]. The results of kinetic parameters obtained for doped and un-doped MnO_x/C are summarized in Table 1, together with those for the benchmark 20 wt.% Pt/Vulcan XC72 (E-Tek).

Estimation of the active surface area (SA) of the MnO_x/C catalysts was approximate because the manganese oxide particles size distribution was unknown. Current densities were thus referred to the geometric electrode area and the mass activities (MA) of the catalysts (Table 1). As a first approximation, all the Mn was assumed to be present as active MnO_2, with a loadings of ca. 20 wt.%. [13]. Also in comparing the data for Pt and Mn/C catalyst in the case of Mn it should be noted that there was half the mass in the active layer. Physico-chemical characterisation of the MnO_x/C-based materials to determine the morphology and chemistry of the manganese oxide particles dispersed on the carbon substrate is part of on-going work.

Kinetic parameters determined from the RDE studies were the Tafel slope in the low current density range, b, and the kinetic current density at 0.0 V vs. SHE (Fig. 3b). The high current density was not considered because the linear zones were poorly defined in the low ORR potential range ($E < -0.2$ V vs. SHE), and the adsorption isotherms of oxygenated species were probably different on the surfaces of manganese oxides and platinum.

The oxidised carbon support showed appreciable activity in the ORR potential range (see the example of $Monarch_{ox}$, Fig. 3b). The presence of oxygenated groups on the surface of the carbon, partially formed by oxidation with permanganate, may facilitate oxygen reduction, as reported by Kinoshita [4]. However, dispersion of manganese oxides onto the high area carbon substrates improved the ORR activity at neutral pH in the low current density range (Fig. 3b). The influence of the carbon substrate was more significant in the case of the carbon $Monarch_{ox}$: indeed, at 0.0 V vs. SHE, the geometric ORR kinetic current densities $|i_k|$ were ca. +0.6 and +1.3 mA $cm^{-2}{}_{geom.}$, for $Monarch_{ox}$ and the MnO_x/Monarch catalyst, respectively (Table 1). The ORR activity of the 20 wt.% Pt/Vulcan XC72 was around 10 times higher than that of manganese oxide: MA were ca. 100 A g_{Pt}^{-1} at 0.0 V vs. SHE compared to 9.0 A $g_{MnO_2}^{-1}$ for MnO_x/Monarch (Table 1). The Pt/Vulcan XC72 catalyst exhibited a lower ORR overvoltage (ca. 0.26 V) than un-doped MnO_x/C electrocatalysts (Table 1, Fig. 4).

For the MnO_x/Vulcan-based catalysts, Ni^{II} doping improved the ORR kinetics in the low current density range; the MA was 9 for Ni-MnO_x/Vulcan, compared to 4 A $g_{MnO_2}^{-1}$ for un-doped MnO_x/Vulcan (Table 1). Doping

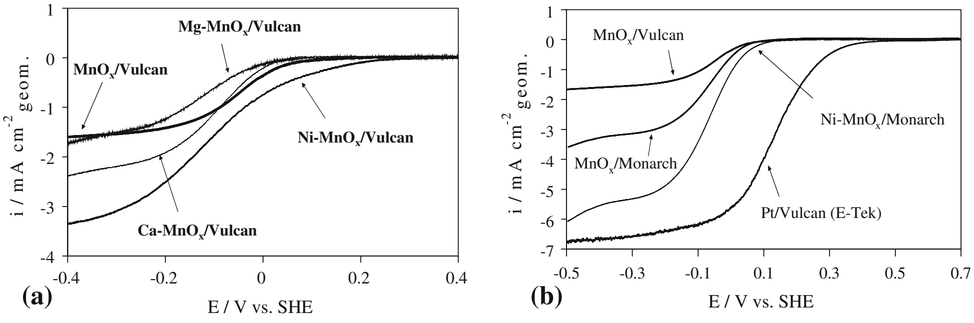

Fig. 4 (**a**) Linear Sweep Voltammograms for the MnO_x/Vulcan-based materials. Scan rate 0.001 V s^{-1}, 2,500 rpm, O_2-saturated 0.1 M Na_2SO_4 solution, 25 °C. (**b**) LSVs for MnO_x/Vulcan, MnO_x/Monarch, Ni-MnO_x/Monarch and the 20 wt.% Pt/Vulcan XC72, 2,500 rpm, O_2-saturated 0.1 M Na_2SO_4 solution, 25 °C, scan rate 0.001 V s^{-1}

with Mg or Ca did not improve the oxygen reduction kinetics: the ORR potential was more negative (−0.11 V) for Ca-MnO_x/Vulcan whilst for Ni-MnO_x/Vulcan it was more positive (+0.06 V). For the Mg-doped catalyst the potential was similar to the un-doped material (Fig. 4). Thus doping by Ni^{II} (or possibly Mg^{II}) may have facilitated decomposition of peroxides. In the case of MnO_x/Monarch-based catalysts, doping by Ni was beneficial, since it significantly increased the ORR activity of the MnO_x/Monarch-based catalysts. Indeed the MA were ca. 19 and 9 A $g^{-1}_{MnO_2}$ (at 0.00 V vs. SHE) for Ni-MnO_x/Monarch and MnO_x/Monarch, respectively, compared with 100 A $g^{-1}{}_{Pt}$ for 20 wt.% Pt/Vulcan XC72 (Table 1). The positive effect of nickel doping on the ORR, has also been reported in alkaline medium and was explained by the ability of transition metal atoms to exist in several valencies [11–13]. Thus the transition metals assist the charge transfer to oxygen, leading to increased electronic interactions with the stabilized Mn^{III} produced from MnO_2 by proton insertion in the ORR potential range.

As a comparison of activity, Yu et al. [5] showed that iron phthalocyanine supported on Vulcan XC72 from E-Tek (FePcVC) exhibited, in 50 mM phosphate buffer medium at pH 7.0, ORR activity close to that of 20 wt.% Pt/Vulcan XC72. The open circuit potential of FePcVC was ca. +0.50 V vs. SHE compared with +0.55 V vs. SHE for the Pt catalyst. Thus based on the relative cost of the catalysts, MnO_x/C materials are promising as non-platinised catalysts for the ORR at neutral pH: the cost of manganese is at least 100 times lower than platinum (in June 2008, according to the New York stock exchange, the cost of platinum was ca. 70 \$ g^{-1}, a ton of ore containing 48% of Mn costing ca. 120 \$).

The stability of the MnO_x/C-based catalysts was good as indicated by the reproducible LSVs in the ORR potential range. The first fuel cell tests using the carbon-supported manganese oxide ORR catalysts produced constant performance, suggesting no loss of active material. Long term (months) of fuel cell testing is needed to assess catalyst stability and will be reported later.

3.4 ORR mechanism

In alkaline solution, the ORR on MnO_x/C involves two competitive pathways [21]: the 4-electron reduction yielding OH^- ions and the 2-electron pathway yielding peroxide ions as intermediates. The number of electrons exchanged per molecule of oxygen reduced on the active layer (n) can be determined, in the ORR potential range, from the Levich slope $B = 0.1\ n$ (see part 3.2). Values of n for the MnO_x/C-based and Pt/Vulcan XC72 (E-Tek) catalysts and the carbon supports, obtained from the experimental Levich slopes (see the examples of MnO_x/Monarch, Fig. 3c), in the ORR potential range at neutral pH, are shown in Fig. 5.

The ORR mechanism was difficult to determine at neutral pH due to resistive effects induced by the low concentration of hydroxide ions in the solution. However from the data, n was close to 2 for the carbon supports, in agreement with previous data for the ORR mechanism on carbon, i.e. a 2-electron reduction yielding peroxides [4]. In the low current density range ($E > -0.2$ V vs. SHE), the value of n (between 2 to 3) for both carbon supports increased with the addition of MnO_x (Fig. 5a): manganese oxides have previously been shown to effectively decompose peroxides [11]. It was likely that the main part of the 2-electron reduction pathway was due to the presence of carbon. In the low current density range the Tafel slopes, were ca. −0.134 and −0.177 V dec^{-1} for MnO_x/Vulcan and MnO_x/Monarch, respectively (Table 1) indicating that the ORR mechanism can be modified by the substrate. This behaviour suggests that the two catalysts had different surface characteristics, as indicated by the limiting currents shown in Fig. 4b, due to functionalisation of the carbon surface, yielding different electronic interactions with O_2 during the ORR. The ORR mechanism on MnO_x/C at neutral pH was different to that in strong alkaline solution, for which the Tafel slope was ca. −0.06 V dec^{-1} in the low current density range [13]. This suggests that at neutral pH more peroxide is formed per molecule of reduced oxygen in the ORR potential range.

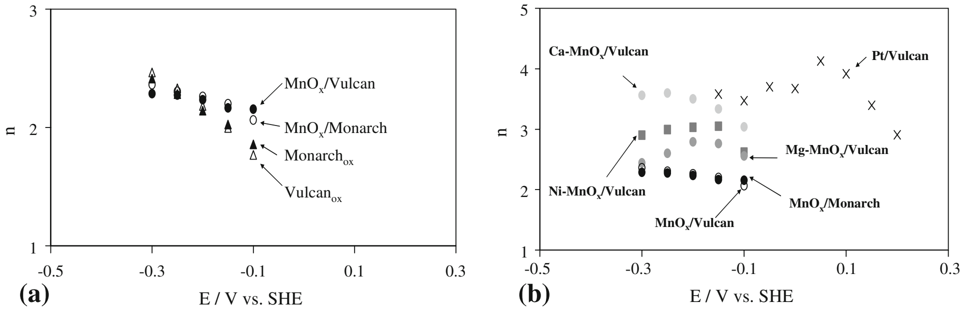

Fig. 5 Variation of number of electrons n with potential in the ORR potential range O_2-saturated 0.1 M Na_2SO_4 solution, 25 °C. (**a**) MnO_x/Vulcan, MnO_x/Monarch, Ni-MnO_x/Monarch and the carbon supports, previously oxidised. (**b**) (MnO_x/C-based catalysts and the benchmark 20 wt.% Pt/Vulcan XC72

The value of n increased with metal ion doping of the carbon-based manganese oxide catalysts (Fig. 5b) in agreement with observations in high pH (alkaline) medium [13]. This was more significant for the Ca-MnO_x/Vulcan catalyst (n between 3 and 4) where doping orientated the ORR mechanism towards the 4-electron reduction pathway and produced fewer peroxide intermediates. Metal insertion increased the inter-plane distance between the manganese oxide layers (such as observed by XRD, see part 3.1) and the probability of water in the lattice and, as a consequence, the dispproponation of peroxides by MnOOH in aqueous medium, leading to an apparent 4-electron oxygen reduction. The presence of water in the MnO_2 lattice has been previously shown for carbon-supported manganese oxide nanoparticles [22]. In that context, calcium doping was more beneficial than nickel or magnesium doping (atomic distance of 180 pm for Ca compared with 150 and 135 pm for Mg and Ni, respectively). However, in the case of MnO_x/Vulcan-based catalysts, the Tafel slope significantly changed with the Ni or Mg doping, whereas with Ca it did not (Table 1). The high values of b, ca. -0.335 and -0.305 V dec^{-1} for Ni- and Mg-MnO_x/Vulcan are, however, questionable as they indicate a very slow oxygen adsorption reaction and/or the blocking of such active layers by either a reaction intermediate (e.g. hydrogen peroxides) or adsorbed anions such as SO_4^{2-}. Increasing electronic interactions, due to the presence of Ni (see part 3.2), may change the oxygen adsorption step on MnO_x/C and lead to greater disproportionation of peroxides by MnOOH [21].

In the case of Monarch-supported manganese oxide nanoparticles, Ni doping did not dramatically change the Tafel slope in the low current density range; i.e. b was ca. -0.177 V dec^{-1} for MnO_x/Monarch (cf. -0.113 V dec^{-1} for Ni-MnO_x/Monarch). However, the value of n was ca. 4 for Ni-MnO_x/Monarch, suggesting the 4-electron ORR mechanism was predominant. This is of great significance for fuel cells where peroxides can lead to corrosion of catalyst supports.

The determination of n from the Levich slopes is not very accurate, especially in the high current density range ($E < -0.2$ V vs. SHE). Rotating ring disc electrode (RRDE) experiments are preferred to determine the percentage of peroxides formed per molecule of reduced oxygen. Overall the ORR mechanism on MnO_x/C materials in neutral pH solution may proceed via two parallel pathways. These are direct 4-electron reduction of O_2 to OH^-, which mainly occurs on manganese oxide particles, and a 2-electron reduction of O_2 yielding HO_2^-, especially on the carbon support, peroxide ions then being decomposed either on the MnO_x/C catalyst or in solution. The MnO_2/MnOOH species may act as an oxygen mediator (acceptor/donor), with the first step of both pathways being proton insertion (2). The divalent metals may facilitate decomposition of HO_2^- on the metal-MnO_x/C, the 4-electron pathway then being more apparent.

4 Conclusions

The ORR on MnO_x/C-based catalysts has been characterised in neutral pH solution using an RDE. These catalysts are promising as cathode materials for microbial fuel cells. The Mn^{III}/Mn^{IV} species can act as mediators in the oxygen reduction mechanism, similar to that proposed in alkaline medium. The doping of manganese oxides by divalent ions enhanced the ORR. The ORR mechanism on MnO_x/C catalysts was either a 4-electron pathway or an indirect 2-electron pathway, yielding peroxides, followed by their decomposition. The metal doping of MnO_x orientated the ORR mechanism towards the 4-electron pathway, yielding less peroxides as intermediates.

Acknowledgments This research was support by the European Union through a Transfer of Knowledge award on biological fuel cells (contract MTKD-CT-2004-517215).

References

1. Gil GC, Chang IS, Kim BH, Kim M, Jang JK, Park HS, Kim HJ (2003) Biosens Bioelectron 18:327
2. Jang JK, Pham TH, Chang IS, Kang KH, Moon H, Cho KS, Kim BH (2004) Process Biochem 39:1007
3. Pham TH, Jang JK, Chang IS, Kim BH (2004) J Microbiol Biotechnol 14:324
4. Kinoshita K (1992) In: Electrochemical oxygen technology. Wiley, New York
5. HaoYu E, Cheng S, Scott K, Logan B (2007) J Power Sources 171:275
6. Clauwaert P, Van der Ha D, Boon N, Verbeken K, Verhaege M, Rabaey K, Verstraete W (2007) Environ Sci Technol 41:7564
7. Nguyen Cong H, Chartier P, Brenet J (1977) J Appl Electrochem 7:383–395
8. Heller-Ling N, Poillerat G, Koenig JF, Gautier JL, Chartier P (1994) Electrochim Acta 39:1669
9. Calegaro ML, Lima FHB, Ticianelli EA (2006) J Power Sources 158:735
10. Bezdička P, Grygar T, Klápště B, Vondrák J (1999) Electrochim Acta 45:913
11. Klápště B, Vondrák J, Velická J (2002) Electrochim Acta 47:2365
12. Vondrák J, Klápště B, Velická J, Sedlaříková M, Reiter J, Roche I, Chainet E, Fauvarque JF, Chatenet M (2005) J New Mater Electrochem Syst 8:209
13. Roche I, Chainet E, Chatenet M, Vondrák J (2007) J Phys Chem C 111:1434
14. Roche I (2007) Thèse de doctorat, INPG
15. Zhang XG, Shen CM, Li HL (2001) Mater Res Bull 36:541
16. Warren BE (1990) In: X-ray diffraction. Dover Publications, Dover, New York, p 251
17. Pourbaix M (1963) In: Atlas d'équilibres électrochimiques. Gauthier-Villard, Paris

18. Kozawa A, Yeager JF (1965) J Electrochem Soc 112:959
19. Diard JP, Le Gorrec B, Montella C (1996) In: Cinétique Electrochimique. Herman, Paris
20. Gloaguen F, Andolfatto D, Durand R, Ozil P (1994) J Appl Electrochem 24:863
21. Mao L, Zhang D, Sotomura T, Nakatsu K, Koshiba N, Ohsaka T (2003) Electrochim Acta 48:1015
22. Roche I, Chainet E, Chatenet M, Vondrák J (2008) J Appl Electrochem (in press)